Effect of Stress State on the Stress-Induced Martensitic Transformation in Polycrystalline Ni-Ti Alloy

KURT JACOBUS, HUSEYIN SEHITOGLU, and MARK BALZER

The effect of stress state on the character and extent of the stress-induced martensitic transformation in polycrystalline Ni-Ti shape memory alloy has been investigated. Utilizing unique experimental equipment, uniaxial and triaxial stress states have been imposed on Ni-Ti specimens and the pseudoelastic transformation strains have been monitored. Comparisons between tests of differing stress states have been performed using effective stress and effective strain quantities; a strain offset method has been utilized to determine the effective stress required for transformation under a given stress state. Results of the tests under different stress states indicate that (1) despite the negative volumetric strain associated with the austenite-to-martensite transformation in Ni-Ti, effective stress for the onset of transformation decreases with increasing hydrostatic stress; (2) effective stress *vs* effective strain behavior differs greatly under different applied stress states; and (3) austenite in Ni-Ti is fully stable under large values of compressive hydrostatic stress.

I. INTRODUCTION

To successfully model and utilize the mechanical behavior of Ni-Ti, the governing stress-induced martensitic transformation must be thoroughly understood. The present investigation has sought to further the current understanding of the stress-induced martensitic transformation in Ni-Ti by applying unique triaxial stress states to polycrystalline Ni-Ti and measuring the resulting pseudoelastic transformation strains. The results presented in this work are currently being used in the development of new models for the thermomechanical behavior of materials exhibiting stress-induced martensitic transformations.

A number of previous investigations have considered the effect of stress state on the stress-induced martensitic transformation. A large portion of these investigations have focused on the effect of hydrostatic compression on the martensitic start (M_s) and austenite start (A_s) temperatures. In the study of martensites exhibiting a negative volumetric transformation strain, *i.e.*, $\Delta V^{tr} = V_m - V_a < 0$, linear increases in transformation temperature with increasing hydrostatic pressure have been observed in Au-Cd,[1] Cu-Al-Ni,[2] and the R phase to M phase transformation in Ni-Ti.[3] For the austenite to R phase transformation in Ni-Ti, which exhibits no volume change ($\Delta V^{tr} = 0$), transformation temperatures have been found to remain constant with increasing hydrostatic pressure.[3] Finally, for the positive volumetric change ($\Delta V^{tr} > 0$) transformation observed in Fe-Ni-Co-Ti, transformation temperatures have been found to decrease with increasing hydrostatic pressure.[3] The results of these studies indicate that the effect of pressure on martensitic transformation is linked to the volumetric change ($\Delta V^{tr} = V_m - V_a$) associated with the austenite (parent) to martensite transformation, *i.e.*, hydrostatic pressure favors transformations that result in a negative volumetric change and hinders those that result in a positive volumetric change.

Research efforts have also focused on stress-induced transformations that occur when an effective stress component is present. The influence of uniaxial stress sense (tension *vs* compression) on the pseudoelastic stress-induced martensitic transformation has been examined to a limited extent. Although some treatments have found strong symmetry between tension and compression behavior for Au-Cd single crystals,[4,5] the majority of the treatments find at least some degree of asymmetry between tensile and compressive behavior. Burkart and Read[6] studied the stress-induced transformation in In-Tl single crystals and found that at a given temperature, 20 pct more compressive stress than tensile stress was needed to begin the transformation. Sakamoto *et al.*[7] reported significantly higher transformation stresses in tension than in compression in Cu-Al-Ni single crystals and hypothesized that the result was due to formation of different product phases under tension and compression. More recently, Vacher and Lexcellent[8] relayed results for polycrystalline Cu-Al-Ni in strong agreement with those of Burkhart and Read: higher stresses were required for the onset of transformation in compression than in tension. A similar result was observed in polycrystalline Ni-Ti.[9] Patoor *et al.*[10] noted that a larger number of variants were available in tension *vs* compression and developed a micromechanical model on this basis. It should be mentioned that there are currently no studies available in which both effective and hydrostatic stresses were systematically changed.

Before discussing experimental details, we give a brief background on the Ni-Ti alloy system. As with any shape memory alloy, Ni-Ti owes its unique behavior to the stress-induced martensitic transformation. A necessary precondition for the stress-induced martensitic transformation is the retention of a metastable austenite phase. In the case of near $Ni_{50.0}Ti_{50.0}$ at. pct alloy, this austenite phase takes the form of an ordered bcc superlattice (designated B2) β phase with $a \approx 3$ Å.[11,12] With sufficient cooling and/or stress, the β phase in Ni-Ti will, in a diffusionless and shear dominated reaction, transform to a martensite phase of different crystal

KURT JACOBUS and MARK BALZER, Graduate Research Assistants, and HUSEYIN SEHITOGLU, Professor and Associate Head, are with the Department of Mechanical and Industrial Engineering, University of Illinois at Urbana–Champaign, Urbana, IL 61801.

Manuscript submitted February 27, 1996.

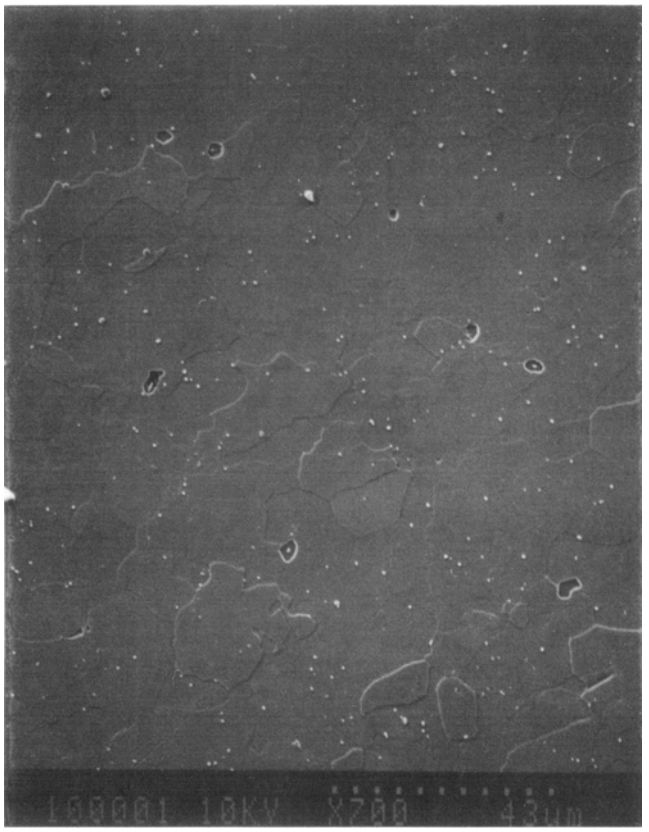

(*a*)

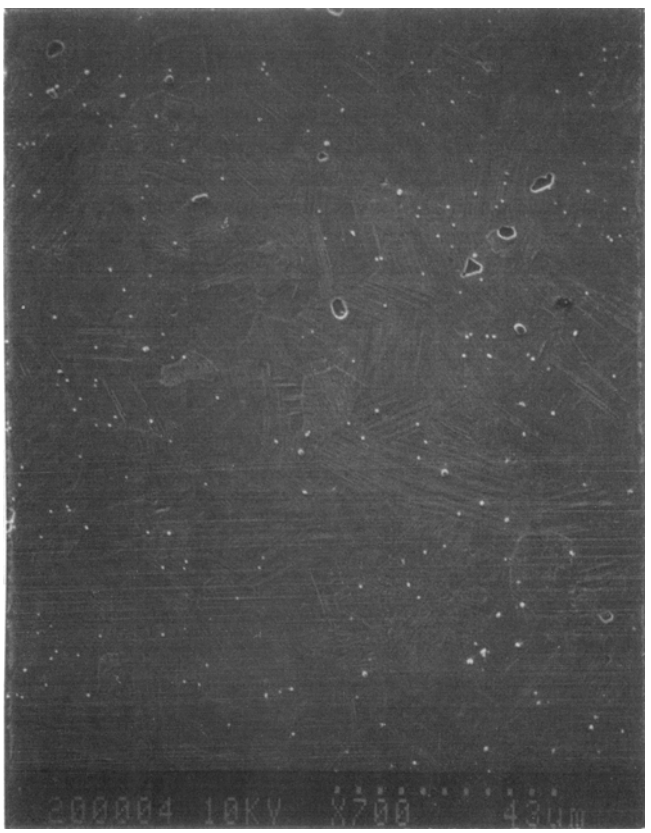

(*b*)

Fig. 1—(*a*) Typical microstructure of Ni-Ti specimens showing grain boundaries in the austenite phase; (*b*) typical microstructure of Ni-Ti specimen subjected to uniaxial tension showing the martensitic phase.

structure. It is accepted that the Ni-Ti martensite is a monoclinic distortion of a B19 lattice ($a \approx 2.883$ Å, $b \approx 4.623$ Å, $c \approx 4.117$ Å, and $\gamma \approx 96.8$ deg).[13,14] Calculations based on the lattice parameters of the austenite and martensite crystal structures in Ni-Ti indicate that the austenite-to-martensite transformation in Ni-Ti results in a shear strain, g, of 0.13 and a volume change, $\Delta V^{tr}/V$, of -0.0034.[15]

A very limited range of compositions is capable of producing the ordered bcc austenite structure necessary for stress-induced martensitic transformations in Ni-Ti. The practical compositional limits for Ni-balance alloys are 49 to 51 at. pct Ti. In this compositional range, transformation temperatures from −200 °C to 110 °C can be achieved depending upon heat treatment.[16]

With this background, the purpose of the present investigation of Ni-Ti is

(1) to determine the transformation stress in tension, compression, and under varying levels of effective stress when hydrostatic stress levels are highly compressive (~1 GPa);
(2) to establish the stress-strain behavior beyond the initial transformation stress;
(3) to critically discuss the capabilities and limitations of the proposed stress-strain models of pseudoelastic deformation in view of the experimental findings; and
(4) to demonstrate a novel apparatus that can apply variable axial and lateral loads simultaneously.

II. EXPERIMENTAL TECHNIQUES

$Ni_{50.0}Ti_{50.0}$ at. pct alloy was employed for all experimental work. The alloy was purchased from Special Metals Inc. (New Hartford, NY) and was heat treated by Memry Corporation (Brookfield, CT).

All Ni-Ti specimens were prepared in a single batch. Tensile specimens were prepared with a nominal gage length of 25.4 mm and a gage diameter of 7.37 mm; compression specimens had a nominal gage length of 19.05 mm and a gage diameter of 11.13 mm. Triaxial pressure specimens were prepared with a nominal gage length of 12.7 mm and gage diameter of 5.59 mm. The heat treatment for all specimen designs consisted of soaking at 550 °C for 15 minutes followed by a water quench to ambient temperature; heat treatment was selected to avoid the *R*-phase transformation. This was verified by differential scanning calorimetry.[17] The resultant microstructure was polycrystalline with an average grain diameter of 19 μm; a micrograph is provided in Figure 1. All bars were heat treated prior to machining and differential scanning calorimetry was performed on Ni-Ti specimen blanks. Ni-Ti samples were tested between temperature limits of −70 °C and +70 °C; samples were heated/cooled at a rate of 10 °C/min. Average transformation temperatures were as follows: $A_f = 8.6$ °C, $A_s = -0.3$ °C, $M_s = -18.1$ °C, and $M_f = -34.2$ °C.

Uniaxial loading of Ni-Ti was performed on an Instron 1331 servohydraulic test machine operating in axial strain control. For tensile tests, a 25.4-mm extensometer was used to monitor axial strains and a diametral extensometer was used to monitor specimen diametral strains. For compression tests, axial and diametral strains were monitored by electrical resistance metal foil strain gages bonded to the specimen gage section. Test definition, command genera-

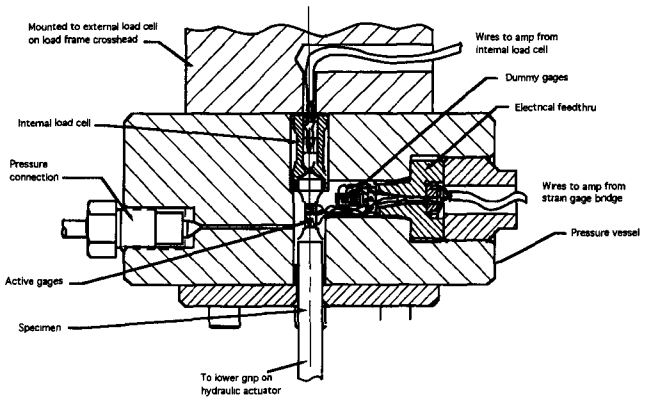

Fig. 2—Sectional view of pressure test chamber, assembled for testing.

Table I. Experimental Stress States

UT	$\sigma_{ij} = \begin{bmatrix} \sigma & 0 & 0 \\ & 0 & 0 \\ & & 0 \end{bmatrix}$
UC	$\sigma_{ij} = \begin{bmatrix} -\sigma & 0 & 0 \\ & 0 & 0 \\ & & 0 \end{bmatrix}$
HC	$\sigma_{ij} = \begin{bmatrix} -\sigma & 0 & 0 \\ & -\sigma & 0 \\ & & -\sigma \end{bmatrix}$
ZH	$\sigma_{ij} = \begin{bmatrix} 2\sigma & 0 & 0 \\ & -\sigma & 0 \\ & & -\sigma \end{bmatrix}$
TC	case I $\sigma_{ij} = \begin{bmatrix} -3\sigma & 0 & 0 \\ & -\sigma & 0 \\ & & -\sigma \end{bmatrix}$
	case II $\sigma_{ij} = \begin{bmatrix} -2\sigma & 0 & 0 \\ & -\sigma & 0 \\ & & -\sigma \end{bmatrix}$

tion, and data collection for both tensile and compressive tests were accomplished *via* personal computer.

An MTS servohydraulic test machine fitted with a unique high pressure vessel was used for triaxial testing of Ni-Ti specimens. The schematic of the test system is provided in Figure 2. As Figure 2 indicates, axial stresses were applied to the specimen by the servohydraulic actuator of the MTS test machine; diametral stresses were applied to the specimen through the introduction of pressurized fluid into the pressure vessel. Specimen strains (axial and diametral) were monitored by a pair of foil strain gages bonded to the specimen gage section; pressure effects on the strain gage output were eliminated by wiring a strain gaged dummy specimen into the bridge circuit inside the vessel. A miniature strain gage load cell placed in the top section of the pressure vessel was used to measure axial specimen load; diametral specimen pressure was monitored by a pressure transducer.

Control of the high pressure testing setup was accomplished with two independent control loops—one for the MTS axial actuator and a second for the servohydraulic pressure intensifier. The independent control loops allow for the application of any desired axial stress/lateral stress ratio within load and specimen stability limits. The ability of the present triaxial testing apparatus to simultaneously ramp the lateral and axial stresses on the specimen represents one of its main advantages over previous triaxial research efforts. In previous works, hydrostatic compression was typically applied first and the uniaxial stress was increased in a secondary operation. The present scheme circumvents any arguments regarding the role of initial hydrostatic compression on the material behavior.[18] A personal computer was used for all test definition, command generation, and data acquisition tasks. More details of the pressure intensifier, load, and strain measurements can be found in a recent publication.[19]

To allow for meaningful comparisons between uniaxial and triaxial tests, the loading rates in the triaxial tests were selected such that they imposed effective strain rates in the elastic regime equivalent to those utilized in the uniaxial tests: 10^{-4} s^{-1}. Transformation stresses, $\sigma_{A \to M}$, required to bring about the austenite-to-martensite transformation under test conditions were determined from the axial stress *vs* axial strain (effective stress *vs* effective strain) using a 0.001 strain offset.

For all tests, stress and strain data were converted from the engineering quantities collected in raw form to true stresses and strains. True strains were computed from engineering strains:

$$\varepsilon_1 = \ln (1 + e_1),\ \varepsilon_2 = \ln (1 + e_2) \qquad [1]$$

Axial true stresses (σ_1) were developed from the engineering stress (S_1) using the following approximate relationship (lateral stresses were collected in "true" form and thus no conversion was necessary):

$$\sigma_1 = \frac{S_1}{(1 + e_2)^2} \qquad [2]$$

where e_2 is the instantaneous diametral engineering strain. Triaxial stresses and strains were converted to effective stresses and strains to allow for comparison with the uniaxial data. The definitions for effective stress and effective strain used for these calculations are given in Eqs. [3] and [4].

$$\sigma_{\text{eff}} = \frac{\sqrt{2}}{2} [(\sigma_1 - \sigma_2)^2 + (\sigma_1 - \sigma_3)^2 + (\sigma_2 - \sigma_3)^2]^{1/2} \qquad [3]$$

$$\varepsilon_{\text{eff}} = \frac{\sqrt{2}}{3} [(\varepsilon_1 - \varepsilon_2)^2 + (\varepsilon_1 - \varepsilon_3)^2 + (\varepsilon_2 - \varepsilon_3)^2]^{1/2} \qquad [4]$$

III. EXPERIMENTAL RESULTS

The present work is concerned with the mechanical behavior of $Ni_{50.0}Ti_{50.0}$ at. pct alloy heat treated to produce pseudoelastic behavior at room temperature.

A summary of experimental conditions is provided in Table I. Note that five distinctly differing stress states were investigated: uniaxial tension (UT), uniaxial compression (UC), hydrostatic compression (HC), zero hydrostatic stress (ZH), and triaxial compression tests (TC; cases I and II). For each of these applied stress states,* the axial and di-

*With the exception of the uniaxial tensile tests in which strain control was utilized.

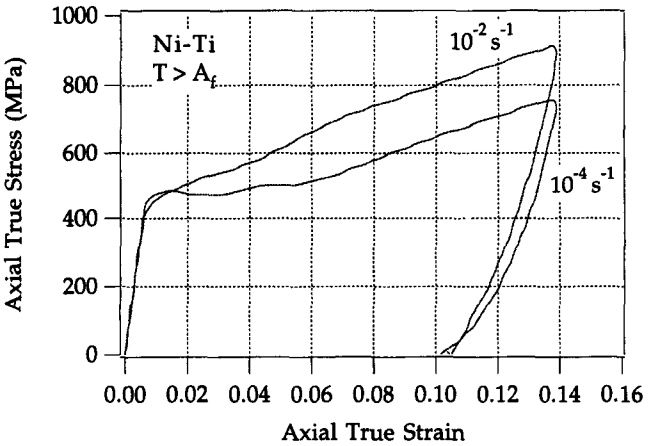

Fig. 3—Effect of strain rate on uniaxial tensile behavior.

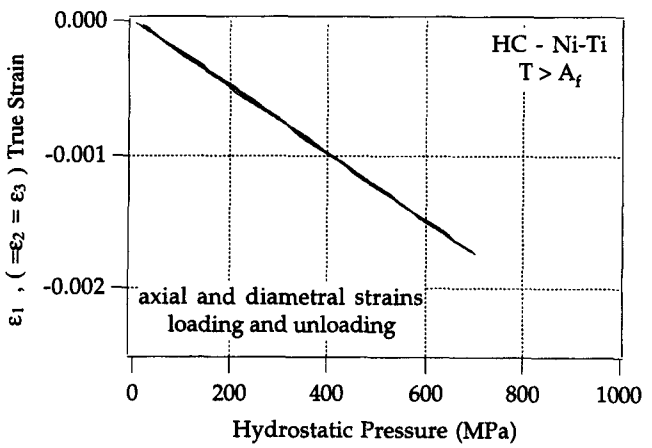

Fig. 4—HC stress state, true axial, and diametral strain *vs* hydrostatic pressure.

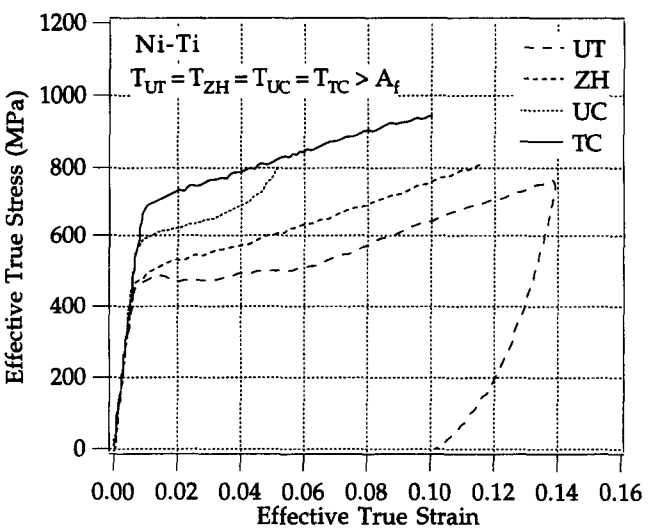

Fig. 5—Summary of experimental results indicating the role of hydrostatic stress in the stress-strain behavior.

ametral stresses were applied to the specimen by starting at a zero stress initial condition ($\sigma = 0$) and then linearly ramping the stress until either the specimen failed or the machine loading limit was achieved. Thus, for the "ZH" condition, the specimen was subjected to simultaneous axial stress and lateral pressure such that the axial stress was tensile in sign and equal to twice the applied instantaneous lateral pressure.

In order to understand the effect of strain rate on mechanical behavior and to assess its influence in the stress-controlled triaxial tests, strain-controlled uniaxial tensile tests with strain rates differing by two orders of magnitude were performed (10^{-4} and 10^{-2} s^{-1}). The results of these tests are provided in Figure 3. As Figure 3 indicates, the stresses for the onset of transformation are nearly the same for the different strain rates. The major difference arises in the postyield transformation region where the high strain rate test shows linear hardening during transformation and the low strain rate test undergoes transformation at a nearly uniform value of stress. The linear hardening observed in the 10^{-2} s^{-1} case is commensurate with the temperature rise during the transformation (measured to be approximately 8 °C) and the resulting increase in stress required to begin the transformation at the higher temperature. Corroborating results have been reported by previous researchers.[20,21] A nearly constant transformation stress was observed in the low strain rate experiment where the temperature change was found to be negligible. Aside from the difference in hardening behavior in the transformation region, the results for the two strain rates are quite similar. Note that the elastic behavior and the hardening modulus in the plasticity dominated region ($\varepsilon_1 > 0.06$) are in strong agreement for the differing strain rates.

We first discuss the HC experiment in which the specimen is loaded under identical compressive stress in both the axial and diametral directions. Results from this test are provided in Figure 4. Under this hydrostatic stress state, linear elasticity predicts the following strain component in all directions:

$$\varepsilon = \frac{-\sigma(1 - 2\nu)}{E} \qquad [5]$$

Note that Eq. [5] predicts a linear change of strains in all directions and identical paths in loading and unloading. As observed in Figure 4, the specimen behavior displays all of these characteristics as well as a slope nearly identical to that computed using average values for elastic modulus and Poisson's ratio (E = 72 GPa, ν = 0.420) gathered from earlier uniaxial tests. As such, it can be concluded that the behavior of the specimen up to a hydrostatic pressure of 700 MPa is fully elastic and thus no transformation behavior is observed. Therefore, hydrostatic pressure of 700 MPa is unable to induce the martensitic transformation in polycrystalline Ni-Ti.

A comparison of representative data from the four remaining stress states (UT, UC, ZH, and TC) is provided in Figure 5 and 6. Initially, in Figure 5, we note that the shapes of the curves beyond yielding differ greatly from test to test. These differences are partly the result of the different strain rates imposed beyond yielding (due to the stress-controlled nature of the testing apparatus) and their effect on the stress-strain behavior. For this reason, we focus our attention on the small strain regime (Figure 6), where effective strain rates are nearly identical, and examine the effect of the imposed stress state on the stress required for transformation. Using a 0.001 strain offset, we find that the UT stress state yields first at 422 MPa, followed by the ZH stress state at 458 MPa, the UC stress

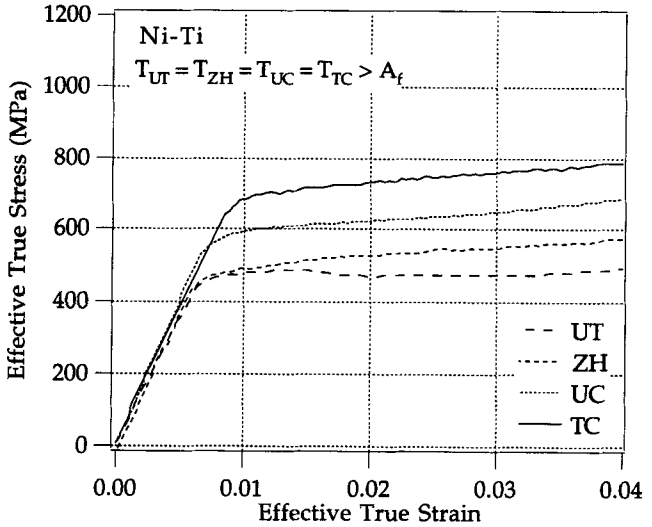

Fig. 6—Replot of Fig. 5 focusing on small strain regime.

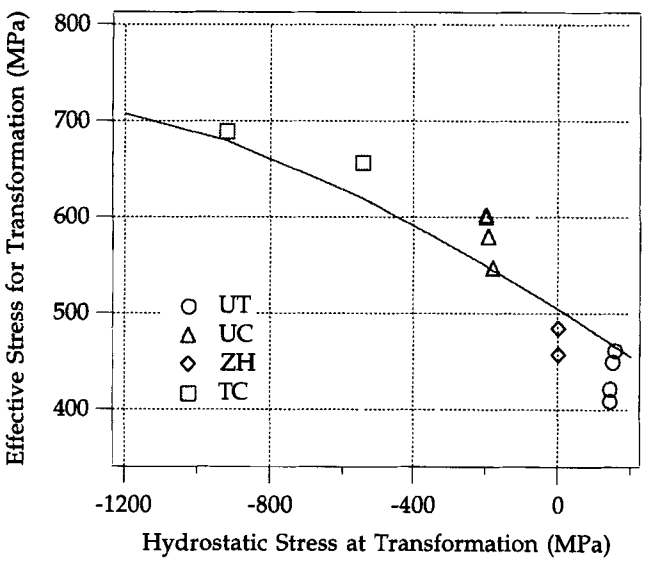

Fig. 7—Effective stress for transformation as a function of hydrostatic stress component at transformation for differing stress states at 20 °C.

state at 548 MPa, and finally the TC stress state at 658 MPa. Thus, the general trend of increasing effective stress for transformation with decreasing hydrostatic component is observed. This trend is displayed in detail in Figure 7 for the imposed stress states; the data is well described by the fitted curve. Note that the tension-compression yield asymmetry is particularly striking.

To gain further insight into the results, representative stress-strain curves from the UT and UC experiments are shown in Figure 8. In the figure, deformation to strains beyond 0.10 (10 pct) is shown, including unloading behavior to zero stress. We note that when the deformation is driven past the maximum transformation strain (~0.06), plasticity becomes the dominant mechanism and that strains are essentially nonrecoverable. Again, we note the enormous tension-compression asymmetry.

The results of these and other experiments are shown as a function of temperature in Figure 9. We note that the flow strength (measured as 0.001 offset) over the temperature range $M_s \leq T \leq M_s^\sigma$ increases with increasing temperature as predicted by the Clausius–Clapeyron relationship. The

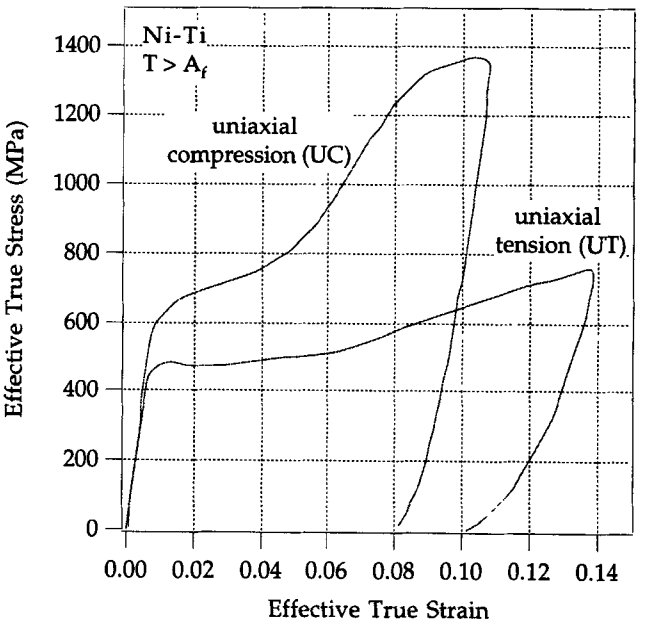

Fig. 8—Comparison of Ni-Ti behavior under UT and UC.

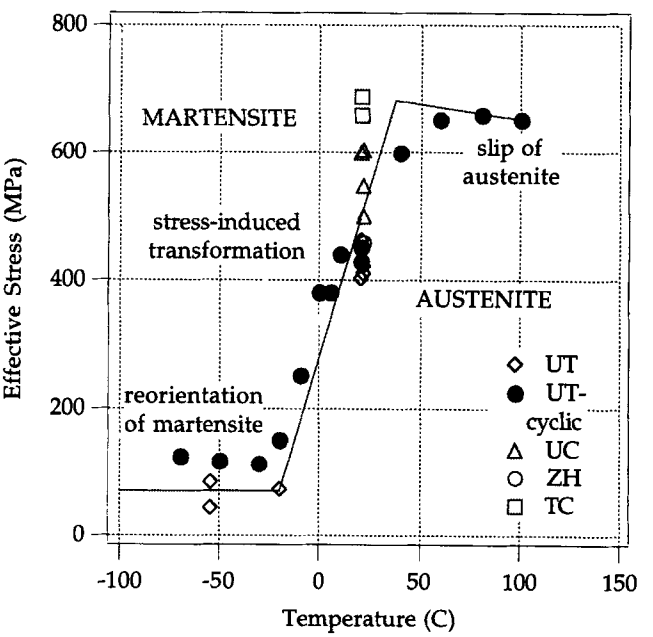

Fig. 9—Variation of effective stress for transformation *vs* temperature showing the increase in stress required for transformation with increasing temperature.

slope, $d\sigma_{eff}/dT$, is nearly 8 MPa/°C which is in general agreement with previous research.[16] At elevated temperatures, $T \geq M_s^\sigma$, *i.e.*, $T \geq 50$°C, the purely austenite specimen deforms by slip and the yield strength decreases with increasing temperature. At temperatures below M_f, $T \leq -34$ °C, the flow stress (0.001 offset) is approximately constant. In this regime, the thermally induced martensite undergoes reorientation (detwinning) under stress.

Finally, it should be mentioned that during the UT experiment, both the axial and diametral strain were monitored, and by removing the elastic volumetric strain, it is possible to gain an understanding of the overall volume change during these experiments. To a first good approximation, the volumetric portion of the macroscopic trans-

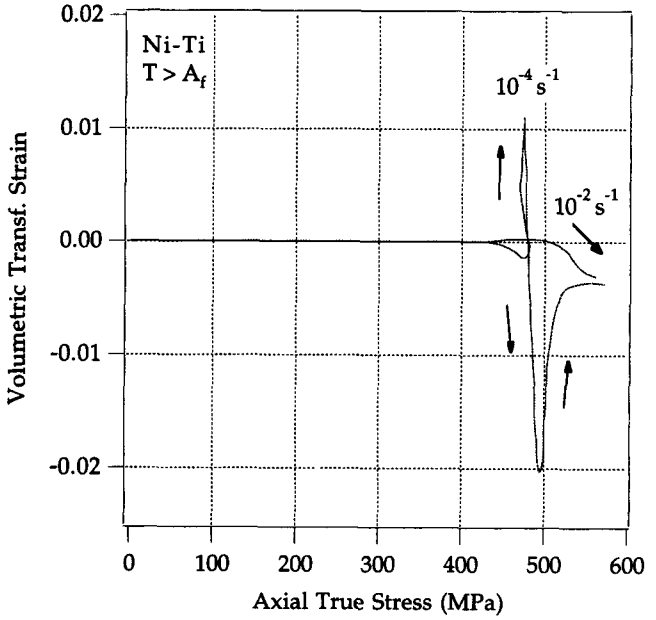

Fig. 10—Development of volumetric transformation strains under high and low strain-rate uniaxial tension.

formation strain is given as[22]

$$\frac{\Delta V^{tr}}{V} = \varepsilon_1 + \varepsilon_2 + \varepsilon_3 - \sigma_1 \left[\frac{(1 - 2\nu)}{E}\right] \qquad [6]$$

In our case, ε_2 and ε_3 are equal and σ_1 represents the applied stress in the axial direction. In Figure 10, we see that for the low and high strain-rate uniaxial tests, the values of volumetric transformation strain upon completion of the stress-induced transformation were found to be -0.0037 and -0.0031, respectively. It is noted that these values are in exceptionally strong agreement with the expected value of -0.0034 calculated from lattice constants.

IV. DISCUSSION OF RESULTS

Since the groundbreaking criterion for the effectiveness of applied stress on the martensitic transformation was proposed by Patel and Cohen,[23] numerous models have been proposed in the literature to describe all aspects of the martensitic transformation. Several of these models have focused solely on the stress-induced martensitic transformation; some of these will be reviewed here in light of the present experimental results on stress state effects.

One of the most comprehensive models of recoverable transformations is that of Sun and Hwang.[24-26] In their model, Sun and Hwang treat the martensite as a spherical inclusion sustaining a uniform transformation shear strain denoted by g. Scaling the transformation strain in each grain relative to this uniform transformation shear strain, g, they develop constitutive equations that can predict the pseudoelastic behavior for three-dimensional loading cases. These constitutive relations predict nearly the same stress for transformation and the same hardening moduli in tension and compression and thus do not accurately describe the present experimental results. It should be mentioned that an earlier version of their model[25] incorporated the volumetric transformation strain resulting from the transformation, but this model is unable to predict the considerable increases in strength with increasing hydrostatic compression reported here.

Other recently proposed models, *e.g.*, Boyd and Lagoudas[27], can potentially predict the effects of volume change on stress-strain response but also are not expected to reproduce the high levels of tensile-compressive asymmetry reported here. Note that all discussions by Lagoudas *et al.* have been confined to the tensile loading regime.

The micromechanical models of Hwang–Lagoudas and coworkers predict a flow criterion of the basic form

$$\frac{\sqrt{3}}{3} g\sigma_{\text{eff}} + \left(\frac{\Delta V^{tr}}{V}\right) \sigma_{\text{H}} - C(T) = 0 \qquad [7]$$

where $\Delta V^{tr}/V$ is the volumetric transformation strain, g is the lattice shear transformation strain, and $C(T)$ includes the chemical free energy associated with austenite-to-martensite transformation $\Delta G_{A\to M}$, a surface energy term, an energy dissipation term, and an internal stress (interaction) term. This equation predicts that hydrostatic pressure favors transformations that result in a negative volumetric change and hinders those that result in a positive volumetric change. This is contrary to the experimental findings reported in this study.

If in Eq.[7] only the chemical free energy term is retained in $C(T)$, as in the classical Clasius–Clapeyron treatment, and if we consider the loading condition where $\sigma_H/\sigma_{\text{eff}} = c$ = constant, the change in effective stress with temperature is

$$\frac{d\sigma_{\text{eff}}}{dT} = \frac{\dfrac{d\Delta G_{A\to M}}{dT}}{\dfrac{\sqrt{3}}{3} g + c\left(\dfrac{\Delta V^{tr}}{V}\right)} \qquad [8]$$

Note that for the experiments conducted in this study, the c values are constant. For UT, $c = 1/3$; for UC, $c = -1/3$; for ZH, $c = 0$; and for TC case I, $c = -5/6$. Equation [8] predicts the correct trends for steels,[27] namely, when the $\Delta V^{tr}/V$ is positive, the $d\sigma_{\text{eff}}/dT$ (the slope of the Clausius–Clapeyron equation) increases as c becomes negative (*i.e.*, when σ_H is negative). In Ni-Ti, the volume change is negative (~ -0.0034); consequently, this treatment predicts that $d\sigma_{\text{eff}}/dT$ for the TC case is lower than the ZH and UT cases. Unfortunately, this is not the correct trend in view of the experiments reported here. Other explanations must be found to explain the experimental trends. The effect of internal stresses (interaction term), when accounted for in the $C(T)$ expression, results in terms in the numerator of Eq. [8] that change as dE/dT, g^2, and $(\Delta V^{tr}/V)^2$. Our experiments show that dE/dT is positive (=133 MPa/°C) in the range 0 °C to 80 °C. Then, the presence of this interaction term is to decrease $C(T)$ only slightly from the $d\Delta G_{A\to M}/dT$, and thus, the overall trend is left unchanged.

One oversight of the preceding models is that they consider only single variant transformation and thus in no way consider the effect of variant self-accommodation. For a single variant, the transformation shear strain, g, based on lattice calculations is considerably larger than the volumetric component $\Delta V^{tr}/V$. Because multiple martensite variants

form in a self-accommodating manner (*i.e.*, consist of alternative twins), the elastic strain energy is minimized and the effective shear strain over the multiple variants is significantly decreased. Mura[29] showed that in the presence of three twin pairs within a multivariant martensite, the resultant shear strain can be ten times lower than the case of a single variant. Thus, multivariant model formulations are more capable of describing the deformation than the single variant models described previously.

Some proposed models have accounted for multivariant interaction; two such models are those of Patoor *et al.*[10,30] The first model uses the self-consistent method and predicts a large scale tension-compression asymmetry. The computations give the tension-compression asymmetry even with positive, negative, and zero volumetric strain. This finding is intriguing but could not be rationalized at the moment; the authors attribute it to the low symmetry of the martensite phase. The second model is a continuum-based model, utilizing a Prager–Drucker flow surface, incorporating both the J_2 and J_3 (second and third invariants of devaitoric stress) in the flow criteria. This model delivers results that are in close agreement with the self-consistent model and it is considerably simpler than the self-consistent model. We note, however, that although J_3 predicts tension-compression asymmetry (because the sign of J_3 changes), it does not produce any hydrostatic stress effect. It predicts lower flow stresses for the equibiaxial compression case than uniaxial compression, which is also contrary to the hydrostatic stress effect shown here. Moreover, it produces a flow surface that violates convexity for certain stress states which is contrary to intuition.

For future analyses of the stress-induced martensitic transformation, the present experimental results bring to light two additional issues that must be considered to develop an accurate model. First, the issue of tension-compression asymmetry in the plastic behavior of the pure phases must be tackled. This is particularly true in the case of the Ni-Ti martensite, where exceptional tension-compression asymmetries in the plastic behavior of both the stress-induced (Figure 8) and thermally induced martensites were observed. Little tension-compression asymmetry was observed in the plastic deformation of the Ni-Ti austenite. A second issue that must be addressed in future models of the stress-induced transformation is that of the macroscopic martensite phase boundary. As the stress-induced transformation takes place in Ni-Ti, it occurs through the passage of a macroscopic phase boundary through the Ni-Ti austenite. This is the cause of the transient spike in volumetric transformation strain observed in Figure 10. This phenomenon has been discussed extensively by Christian.[31] This phase boundary will require an additional free energy term in the constitutive relations; this issue has been considered previously only by a few researchers.[32]

Since the Ni-Ti material will be used in applications where both tension and compression are expected, it is important to develop simple models to capture the asymmetry.[33] We note that previous attempts to predict the bending behavior of Ni-Ti have not been successful and that the interpretation of bending experiments has been difficult. This is largely due to the tension-compression asymmetry of these materials, but the constraint in the third direction could also play a role. It is clear that the experimental findings in the present work must be addressed fully in any future model expected to predict true material behavior.

V. CONCLUSIONS

The experimental results from polycrystalline specimens of Ni-Ti support the following conclusions.

1. The stress required to begin the stress-induced martensitic transformation in polycrystalline Ni-Ti is significantly greater in uniaxial compression than in uniaxial tension.
2. For a given stress state, the effective stress required to pseudoelastically induce martensite in polycrystalline Ni-Ti increases with decreasing values of hydrostatic stress.
3. Experiments conducted at higher temperatures (~100 °C) in the fully austenitic regime confirm that the tension-compression asymmetry of the austenitic phase alone cannot account for the tension-compression asymmetry observed under pseudoelastic deformation.
4. The remarkable difference in the hardening behavior after the conclusion of transformation for tension and compression cases points out that the martensite flow behavior is distinctly different in tension *vs* compression, at least in the high strain regime.
5. Increasing strain rate increased the stress required to sustain the austenite-to-martensite transformation in polycrystalline Ni-Ti. These increases in stress result from the small temperature rise in the material under high strain rates and are consistent with predictions based on the Clausius–Clapeyron equation.
6. Present constitutive models for stress-induced martensitic transformation are not formulated to predict the influence of the stress state, particularly highly compressive hydrostatic stresses, on deformation behavior.

ACKNOWLEDGMENTS

The research is supported by grants from the Department of Energy, Basic Energy Sciences Division (Germantown, MD) and the National Science Foundation, Mechanics and Materials Program (Arlington, VA). Dr. Ming Wu, Memry Corporation (Brookfield, CT) is also acknowledged for his help.

REFERENCES

1. Y. Gefen, A. Halwany, and M. Rosen: *Phil. Mag.*, 1973, vol. 28, pp. 1-9.
2. T. Kakeshita, Y. Yoshimura, K. Shimizu, S. Endo, Y. Akahama, and F.E. Fujita: *Trans JIM*, 1988, vol. 29, pp. 781-89.
3. T. Kakeshita, K. Shimizu, S. Nakamichi, R. Tanaka, S. Endo, and F. Ono: *Mater. Trans. JIM*, 1992, vol. 33, pp. 1-6.
4. N. Nakanishi, T. Mori, S. Miura, Y. Murakami, and S. Kachi: *Phil. Mag.*, 1973, vol. 28, pp. 277-92.
5. D.S. Lieberman, M.A. Schmerling, and R.W. Karr: *Shape Memory Effects in Alloys*, J. Perkins, ed., Plenum Press, New York, NY, 1975, pp. 203-44.
6. M.W. Burkart and T.A. Read: *Trans TMS-AIME*, 1953, vol. 197, pp. 1516-24.
7. H. Sakamoto, M. Tanigawa, K. Otsuka, and K. Shimizu: *Proc. Int Conf. on Martensitic Transformations*, ICOMAT 79, Cambridge, MA, 1979, pp. 633-38.
8. P. Vacher and C. Lexcellent: *Proc. Mechanical Behavior of Materials IV*, M. Jono, ed., Plenum Press, New York, NY, 1991, pp. 231-36.

9. P. Roumagnac: Ph.D. Thesis, Université Technologique de Compiegne, Compiegne, France, 1993.
10. E. Patoor, M. El Armani, A. Eberhardt, and M Berveiller. *J. Phys IV*, 1995, vol. 5, pp. C2-495-C2-500.
11. A. Nagasawa: *J. Phys. Soc. Jpn.*, 1970, vol. 29, pp. 1386-91
12. J. Perkins: *Met. Forum*, 1991, vol. 4, pp. 153-63.
13. K. Otsuka, T. Sawamura, and K. Shimizu: *Phys Status Solidi A*, 1971, vol. 5, pp. 457-62.
14. R.F. Hehemann and G.D. Sandrock *Scripta Metall*, 1971, vol. 5, pp. 801-05.
15. K. Okamoto, S. Ichinose, K. Mori, K. Otsuka, and K. Shimizu *Acta Metall.*, 1986, vol. 34, pp. 2065-73.
16. T.W. Duerig and A.R. Pelton: *Materials Properties Handbook, Titanium Alloys*, ASM INTERNATIONAL, Metals Park, OH, 1994, pp. 1035-48.
17. M. Wu: Memry Corporation, private communication, Brookfield, CT, 1995.
18. S.V. Radcliffe: *The Mechanical Behavior of Materials under Pressure*, H.Ll.D. Pugh, ed., Elsevier, New York, NY, 1970, pp. 638-79.
19. M. Balzer and H. Sehitoglu. *Experimental Mechanics*, accepted for publication.
20. K. Mukherjee, S. Sircar, and N.B. Dahotre: *Mater. Sci Eng*, 1985, vol. 74, pp. 75-84.
21. P.H. Leo, T.W Shield, and O.P. Bruno: *Acta Metall. Mater.*, 1993, vol. 41, pp. 2477-85.
22. R. Neu and H. Sehitoglu: *Metall. Trans. A*, 1991, vol. 22A, pp. 1491-1500.
23. J.R. Patel and M Cohen: *Acta Metall.*, 1953, vol. 1, pp. 531-38.
24. Q.P Sun and K.C. Hwang: *J. Mech. Phys. Solids*, 1993, vol. 41, pp. 1-17.
25. Q.P. Sun and K.C. Hwang: *J. Mech. Phys. Solids*, 1993, vol. 41, pp. 19-33.
26. Q.P. Sun, K.C. Hwang, and S.W. Yu: *J. Mech Phys. Solids*, 1991, vol. 39, pp. 507-24.
27. J Boyd and D. Lagoudas: *Int. J. Plasticity*, in press.
28. R. Neu and H. Sehitoglu: *Acta Metall*, 1991, vol. 40, pp. 2257-68.
29. T. Mura: *Micromechanics of Defects in Solids*, Kluwer Academic Publishers, Boston, MA, 1991, p. 237.
30. E. Patoor, A. Eberhardt, and M. Berveiller: *Mechanics of Phase Transformations and Shape Memory Alloys*, L.C. Brinson and B. Moran, eds., ASME, New York, NY, 1994, pp. 23-37.
31 J.W. Christian: *Metall. Trans. A*, 1982, vol. 13A, pp. 509-38.
32. R Abeyaratne and J.K Knowles: *J Elasticity*, 1989, vol. 22, pp. 63-80.
33 A.R. Pelton, N. Rebelo, T.W. Duerig, and A. Wick: *Proc. 1st Int Shape Memory and Superelastric Technologies*, A.R. Pelton *et al.*, eds., 1995, pp. 353-58.